International Journal of Nanomedicine

Dovepress
Taylor & Francis Group

Open Access Full Text Article

ORIGINAL RESEARCH

Carrier-Free Nanomedicine Based on Celastrol and Methotrexate for Synergistic Treatment of Breast Cancer via Folate Targeting

Xiaojuan Li[1], Mengxin Zhang[1], Xiaolin Wang[1], Ping Ma[2], Yu Song[1]

[1]School of Pharmacy, Fujian University of Traditional Chinese Medicine, Fuzhou, 350122, People's Republic of China; [2]Research and Development, Hikma Pharmaceuticals USA Inc., Bedford, OH, USA

Correspondence: Yu Song, School of Pharmacy, Fujian University of Traditional Chinese Medicine, Fuzhou, 350122, People's Republic of China, Tel/Fax +86 591 22861135, Email songecho@163.com

Purpose: To address celastrol(Ce)'s efficacy and toxicity challenges in breast cancer, we first developed a carrier-free, self-targeting nanosystem with synergistic anti-tumor action by leveraging methotrexate (MTX)'s intrinsic folate moiety for active tumor targeting.

Methods: Ce-MTX nanoparticles (NPs) were prepared using a solvent precipitation method, with formulation parameters optimized. Characterization included particle size, polydispersity index (PDI), encapsulation efficiency (EE), loading efficiency (LE), and TEM. Drug release was investigated under physiological and tumor-mimetic conditions via a dialysis method. Cellular uptake and in vitro anti-tumor effects were evaluated in A549 and 4T1 cell lines. In vivo, tumor distribution and normal tissue accumulation were analyzed in 4T1 tumor-bearing mice. Anti-tumor efficacy and biosafety were evaluated through tumor growth curves, tumor inhibition rates, body weight changes, organ indices, histological analysis, and serum biochemistry.

Results: The optimized Ce-MTX NPs exhibited a particle size of 90.20 nm, PDI of 0.062, and spherical morphology. The EE and LE were 95.15% and 66.53% for Ce, and 95.74% and 33.6% for MTX, respectively. The NPs demonstrated excellent stability over 7 days. Notably, Ce-MTX NPs exhibited pH-dependent drug release, with accelerated release at pH 5.5. Qualitative and quantitative cellular uptake assays revealed significantly higher uptake of Ce-MTX NPs compared to the free drugs, with enhanced folate receptor-targeting in 4T1 cells. Cytotoxicity assays showed stronger anti-tumor activity of Ce-MTX NPs in 4T1 cells compared to the free drug mixture, thus demonstrating the superior synergistic anti-cancer effects achieved by the nanoparticle formulation. Importantly, in vivo studies confirmed substantial tumor growth inhibition and an excellent biosafety profile.

Conclusion: The carrier-free Ce-MTX NPs demonstrated enhanced stability, tumor targeting, and rapid drug release within tumor cells, significantly improving the efficacy and biosafety of breast tumor treatment. These nanoparticles offer a promising strategy for combined cancer therapy and hold great potential for further development in nanomedicine.

Keywords: celastrol, methotrexate, carrier-free nanoparticles, tumor targeting, breast cancer, synergistic antitumor efficacy

Introduction

Breast cancer has emerged as a critical global health challenge, with increasing incidence and mortality rates, making it a major threat to women's health worldwide.[1] As of now, the main clinical treatment methods for breast cancer include surgery, radiotherapy, and chemotherapy. Among these, chemotherapy plays an essential pivotal role in the comprehensive management of breast cancer. However, conventional chemotherapeutic agents are often limited by poor water solubility, lack of selectivity, or low bioavailability, leading to poor therapeutic outcomes and severe side effects.[2] Compelling clinical evidence indicates that 60–70% of breast cancer patients experience debilitating adverse reactions, ranging from myelosuppression to gastrointestinal and cardiac toxicities, which significantly compromise treatment efficacy and patient quality of life.[3] Therefore, the development of more targeted and effective therapeutic strategies is urgently needed.

Received: 11 January 2025
Accepted: 23 June 2025
Published: 27 June 2025

In recent years, natural product-derived antitumor agents have attracted considerable attention. Celastrol (Ce), a pentacyclic triterpenoid monomer compound extracted from *Tripterygium wilfordii* Hook.f., has demonstrated promising antitumor potential. Current studies have shown Ce's broad-spectrum antitumor activity, with efficacy observed across various tumor types, including prostate cancer,[4] hepatocellular carcinoma,[5] glioma,[6] and breast cancer.[7] Despite its promising antitumor effects, the clinical application remains limited due to significant challenges, including pronounced toxicity, low water solubility (<0.1 μg/mL), minimal bioavailability (<5%), and rapid systemic clearance. Addressing these limitations has become a focus of ongoing research. Recent advancements in nanomedicine formulations, such as liposomes,[8] micelles,[9] microemulsions,[10] and nanoparticles,[11] have opened new avenues for optimizing Ce drug delivery systems. In these nanodelivery systems, drug molecules are either encapsulated within nanoparticles or loaded onto the surface of nanocarriers, and subsequently delivered to the tumor site through active or passive targeting mechanisms to exert its therapeutic effect.[12,13] However, the complexity of preparation, low drug loading capacity, and slow drug release rates of traditional carrier-based nanodelivery systems limit their clinical applicability. Furthermore, since the carrier materials are typically exogenous, there is an associated risk of long-term toxicity.[14–16] To address these challenges, carrier-free nanoparticles have emerged, wherein therapeutic molecules self-assemble via non-covalent interactions (eg, π-π stacking, hydrophobic effects), achieving unprecedented drug loading (approaching 100%) while eliminating excipient-related toxicity. For example, Xiao et al developed a simple, safe, and effective carrier-free nanoparticle formulation combining Ce and doxorubicin to overcome doxorubicin resistance and enhance therapeutic efficacy.[17] However, despite these advantages, the targeting ability of this type of nanosystem still leaves much to be desired.

In this context, methotrexate (MTX), a well-established broad-spectrum antitumor agent, is an ideal candidate for combination therapy.[18–21] MTX inhibits dihydrofolate reductase, disrupting DNA synthesis and cell division in tumor cells.[22] Due to its structural similarity to folic acid(FA), MTX selectively binds to folate receptors on the surface of tumor cells, offering a promising mechanism of targeted therapy.[23] Notably, our preliminary studies have demonstrated a potent synergistic anticancer interaction between Ce and MTX, which can potentially enhance the efficacy of both drugs in breast cancer treatment. Moreover, carrier-free MTX nanoparticles exhibit pH-responsive release profiles,[24,25] primarily due to the increased solubility of MTX in an acidic environment.[24] This pH-dependent release can enhance drug delivery, especially within tumors, improving therapeutic outcomes.[26] Building on these findings, the goal of this study is to develop self-assembled, carrier-free Ce-MTX NPs that exploit the folate receptor targeting mechanisms. This approach aims to increase drug accumulation at tumor sites, enhance synergistic antitumor effects in breast cancer, and reduce systemic side effects. The design and potential applications of Ce-MTX NPs for targeted cancer therapy are illustrated in Figure 1, where Ce and MTX self-assemble into stable carrier-free nanoparticles through intermolecular forces, significantly improving drug uptake in tumor cells via folate receptor-mediated endocytosis, and then achieve pH-responsive drug release to exert their synergistic efficacy. To the best of our knowledge, although previous studies have reported various types of Ce NPs, there is no prior work that has described a carrier-free, folate receptor-targeting, pH-responsive dual-drug nanoassembly that integrates synergism for breast cancer treatment. This work represents the first demonstration of such a multi-mechanistic Ce-MTX nanoassembly.

Experimental Method

Materials

Ce (purity ≥98%) was purchased from Cassese Pharmaceutical Technology Co., Ltd. (Nanjing, China). MTX was obtained from Sangong Bioengineering Co., Ltd. (Shanghai, China). ICG (dye content: 90%) was acquired from Bailiwick Science and Technology Co., Ltd. Sodium hydroxide and methanol were obtained from Sinopharm Chemical Reagent Corporation (Shanghai, China). Thiazolyl blue (MTT) was purchased from Sigma-Aldrich Corporation (St. Louis, MO, USA). RPMI Medium 1640 basic (1X) and Fetal Bovine Serum (FBS) were procured from Gibco Corporation (Grand Island, NY, USA). Trypsin (0.25%) and Phosphate Buffered Saline (PBS) were purchased from HyClone (South Logan, UT, USA). Instrumentation included an electrothermal constant-temperature oscillation water bath (DKZ, China), a laser particle size analyzer(DLS) (380ZLS, Santa Barbara, USA), an FT-IR spectrometer (Nicolet 6700, Thermo Nicolet, USA), a transmission electron microscope (TEM) (JEM 1200EX, JEOL,

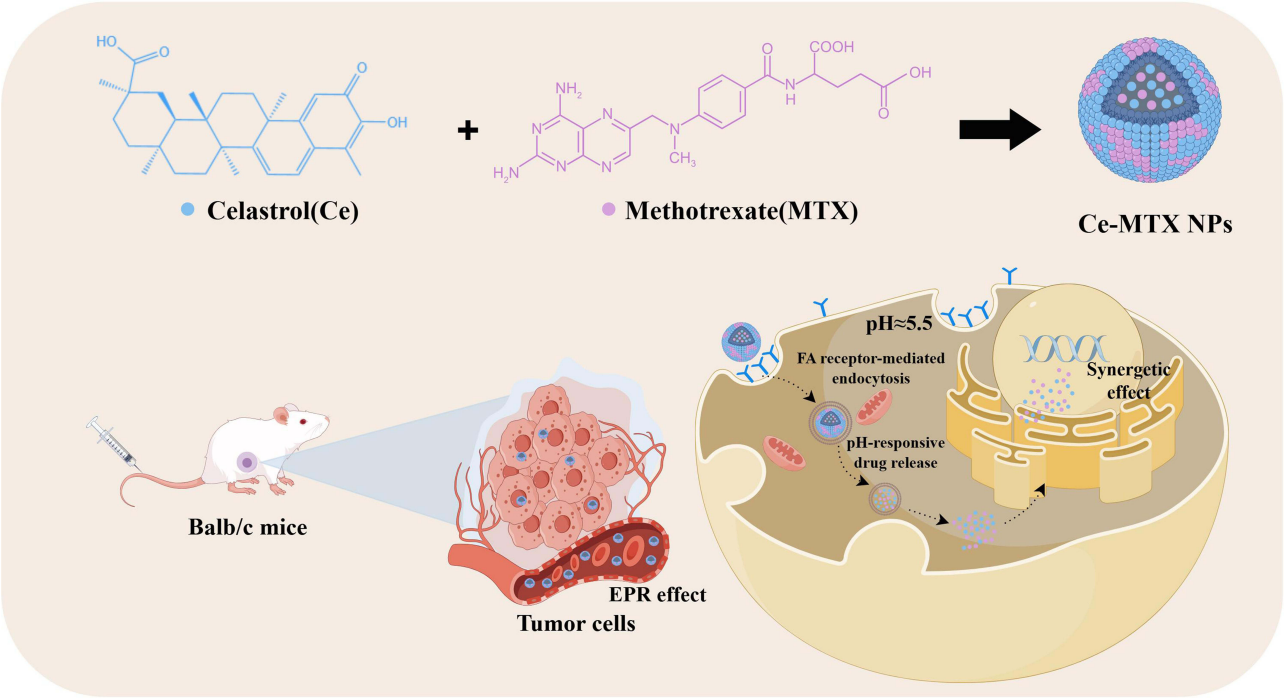

Figure 1 Schematic diagram of Ce and MTX self-assembly into carrier-free nanoparticles for in vivo targeted distribution.

Japan), a high-performance liquid chromatography system (LC 2030, Shimadzu, Japan), a continuous wavelength multifunctional enzyme labeling instrument (M200 PRO, Tecan, Switzerland), a flow cytometer (Agilent Technologies, CA, USA), a confocal laser scanning microscopy (CLSM) (D-35578, Leica, Germany).

Cell Origin

Human lung cancer cells (A549) and mouse breast cancer cells (4T1) were purchased from the Shanghai Cell Bank, Chinese Academy of Sciences.

Preparation of Nanoparticles

To prepare the Ce-MTX NPs, Ce was dissolved in methanol, and MTX was dissolved in NaOH (pH 12), at concentrations of 2 mg/mL and 8 mg/mL, respectively. The Ce solution was then mixed with the MTX solution and stirred for 5 minutes. The mixture solution was slowly added dropwise into a silicon bottle containing 2 mL of ultrapure water, followed by magnetic stirring for 2 hours. The resulting solution was placed on a nitrogen-blowing apparatus at 70°C for approximately 15 minutes, then centrifuged at 3,000 rpm for 15 minutes to remove the free drug.

To optimize the formulation, different solvents were screened for Ce (methanol, anhydrous ethanol, and dimethyl sulfoxide), and their effects on nanoparticle size and PDI were assessed. The mass ratio of Ce: MTX was also varied (1:1, 2:1, 3:1, and 4:1), and its impact on particle size, PDI, EE, and LE was investigated. The formulas for EE and LE are as follows:

$$\mathrm{EE}\ (\%) = \frac{\text{weight of drug in nanoparticles}}{\text{total drug used}} \times 100\%$$

$$\mathrm{LE}\ (\%) = \frac{\text{weight of drug in nanoparticles}}{\text{total weight of nanoparticles}} \times 100\%$$

https://doi.org/10.2147/IJN.S516921

Characterization of Ce-MTX NPs

The particle size and PDI were determined by dynamic light scattering (DLS), after diluting the sample with ultrapure water. Each sample was measured in triplicate, and the average value was calculated. To observe the morphology of the nanoparticles, sample solutions were placed onto a copper grid, stained with 4% phosphotungstic acid solution, and examined under high-resolution transmission electron microscopy (TEM). The UV maximal absorption spectra of Ce-MTX NPs were analyzed using UV-vis spectroscopy and compared with free drug solutions to determine shifts in the UV maximal absorption. Appropriate amounts of free Ce, free MTX, and Ce-MTX NPs were weighed and mixed with KBr, and then ground into a uniform powder. The resulting sample was placed in an infrared spectrometer to obtain the corresponding spectra. To assess the stability of the samples, the solutions were diluted with ultrapure water, PBS (pH 7.4), and RPMI-1640 medium (containing 10% FBS), respectively. The diluted samples were then stored in a refrigerator at 4°C, protected from light. The particle sizes were determined using the DLS at 1-day intervals over 7 days.

Drug Release Test in vitro

Free Ce, free MTX, and Ce-MTX NPs (2 mL each) were securely sealed in dialysis bags (MWCO of 3500 Da) and submerged in 35 mL of PBS buffer solutions (pH 7.4 and 5.5), respectively. The solutions were then placed in a gas-bath thermostatic shaker at 37°C and stirred at 100 rpm. At predetermined time points (0, 1, 2, 4, 8, 12, 24, 48 h), 2 mL of the buffer solution was withdrawn, and an equal volume of fresh buffer solution was added. Ce and MTX concentrations in the samples were quantified by high-performance liquid chromatography (HPLC).

Cell Culture

The A549 and 4T1 cell lines were cultured in RPMI-1640 medium supplemented with 10% FBS and 1% penicillin. The cells were maintained at 37°C in a humidified incubator with 5% CO_2. The medium was replaced every two days.

Cellular Uptake in vitro

To assess the targeting ability of Ce-MTX NPs, Ce-MTX-ICG NPs were prepared by labeling the NPs with indocyanine green (ICG). The uptake behavior of the NPs was evaluated in 4T1 mouse breast cancer cells (high folate receptor expression) and A549 human lung cancer cells (low folate receptor expression). We qualitatively investigated the cellular uptake behavior of different drug groups by confocal laser scanning microscopy (CLSM). Cells were seeded in a confocal dish (3×10^5 cells per well) and cultured overnight to allow adherence. After discarding the culture medium, 1 mL of drug-containing medium (free ICG, folate receptor blocked group, or Ce-MTX-ICG NPs) was added, ensuring an ICG concentration of 2.5 μg/mL. The folate receptor blocking group was incubated with free FA in advance for 2 h, and then Ce-MTX NPs were added for incubation. Cells were incubated at 37°C for 4 hours. After incubation, the culture medium was discarded, and the cells were washed three times with pre-cooled PBS, fixed in 4% paraformaldehyde for 15 min, and then treated with DAPI for 10 min. The cells were evaluated by confocal micro-scopy.

We further quantified the cellular uptake behavior of different drug groups by flow cytometry. Cells were seeded in 6-well plates (5×10^5 cells per well) and cultured overnight to allow adherence. After discarding the culture medium, 2 mL of drug-containing medium was added. Cells were incubated at 37°C for 4 hours. After incubation, the culture medium was discarded, and the cells were washed three times with pre-cooled PBS. The cells were then trypsinized (0.25%) and resuspended in PBS. The cell suspension was transferred to a flow cytometry tube, and the fluorescence intensity was measured using a flow cytometer.

In vitro Cytotoxicity of Ce-MTX NPs

A549 and 4T1 cells in the logarithmic growth phase were seeded in 96-well plates (5×10^4 cells/mL) and allowed to adhere. After medium removal, different concentrations of free Ce, free MTX, Ce+MTX mixture, and Ce-MTX NPs (Ce: 0.25, 0.5, 1, 2, 3 μg/mL; MTX: 0.125, 0.25, 0.5, 1, 1.5 μg/mL) were added and incubated for 24 hours. The medium was then removed, and 100 μL of MTT solution (0.5 g/L) was added. After 4 hours of incubation, the solution was aspirated, and blue formazan crystals were dissolved in 150 μL of DMSO. The absorbance was measured at 570 nm using a microplate reader, and the cell survival was calculated with the following formula:

$$\text{Cell survival rate } (\%) = \frac{OD_{SG} - OD_{BG}}{OD_{CG} - OD_{BG}} \times 100\%$$

Where OD refers to the optical density of the sample group (SG), blank group (BG), and control group (CG). The cytotoxicity experiment was repeated three times.

Combination Index (CI) Analysis

The combination index (CI) was used to evaluate the synergistic effects of Ce and MTX. The CI value was obtained and plotted as a synergistic index using the following formula: $CI = D_a / D_{(x)a} + D_b / D_{(x)b}$. Where D_a and D_b are the concentrations of Ce and MTX that result in a certain degree of cytotoxicity in combination treatment, $D_{(x)a}$ and $D_{(x)b}$ represent the concentration of each drug that produces the same degree of toxicity in monotherapy.

In vivo Distribution

Healthy male BALB/c mice (18–22 g, 6–8 weeks old) were selected to establish a 4T1 hormonal mouse tumor model. All animals used in this study were treated in accordance with the Guidance for the Care and Use of Laboratory Animals. All animal experiments in this study were approved by the Animal Ethics Committee of Fujian University of Traditional Chinese Medicine (The ethics approval number for the use of animals is FJTCM IACUC 2023308). 4T1 cells (1×10^7 cells/mL) were resuspended twice with PBS and inoculated subcutaneously into the right axilla of the mice to induce tumor growth. Once the tumor volume reached approximately 300 mm^3, mice were randomly divided into two groups (n = 3). They were intravenously injected with 200 μL of Ce-MTX-ICG NPs or free ICG (2 mg/kg ICG). Fluorescence imaging was performed at different time points (0 h, 1 h, 2 h, 4 h, 8 h, 12 h, 24 h, and 48 h) using a small animal fluorescence imager. After 48 h, mice were euthanized, and their major organs (heart, liver, spleen, lung, and kidney) were collected, imaged, and analyzed.

Antitumor Assay and Histological Analysis in vivo

Tumor-bearing mice (tumor volume ~100 mm^3) were randomly divided into five groups (n = 6). Mice were intravenously injected with 200 μL of free Ce, free MTX, Ce+MTX mixture, Ce-MTX NPs (3 mg/kg Ce, 1.5 mg/kg MTX), or physiological saline on days 1, 4, 7, 10, and 13, respectively. Tumor volume (in weight) was measured every two days, and the health and body weight of the mice were monitored. At the end of treatment, the mice were euthanized; their blood, major organs, and tumors were collected. Tumor volume (V) was calculated using the formula:

Tumor Volume (V, mm^3) = (long diameter × short diameter^2)/2

Organ Index (%) and tumor inhibition rate (%) were calculated as follows:

Organ Index (%) = (organ weight/mouse weight) × 100%

Tumor Inhibition Rate (%) = (average tumor weight of control group – average tumor weight of treatment group)/average tumor weight of control group × 100%

After weighing, the selected organs (heart, liver, spleen, lung, kidney) and tumor tissues from three mice in each group were fixed in 4% paraformaldehyde solution for 24 hours, embedded in paraffin, and stained with eosin and hematoxylin for histological analysis. The collected serum samples were stored in a −20°C freezer for further analysis. The levels of four indicators – alanine aminotransferase (ALT), aspartate aminotransferase (AST), creatinine (CRE), and blood urea nitrogen (BUN)- were measured in mice using an ELISA detection kit. The resulting data were statistically analyzed to evaluate the extent of liver and kidney damage caused by Ce-MTX NPs.

Statistical Analysis

All data are expressed as mean ± standard deviation (SD). Statistical analysis was performed using Origin 2021 64-bit and GraphPad Prism 9.0. One-way analysis of variance (ANOVA) was used to assess the significance of differences between groups. A p-value of < 0.05 was considered statistically significant.

Results and Discussion

Preparation and Optimization of Ce-MTX NPs

The size of nanoparticles plays a crucial role in their ability to penetrate into tumor cells. As shown in Table 1, the smallest carrier-free nanoparticles were obtained when methanol was used as a solvent. This may be attributed to a high dielectric constant and lower hydrogen bonding of methanol compared to other solvents, which causes slower changes in the polarity of the solvent mixture, resulting in smaller particle sizes.[27] Therefore, methanol was selected as the optimal solvent for Ce-MTX preparation. Table 2 summarizes the results of mass ratio optimization for Ce to MTX, ranging from 1:1 to 4:1. The optimum mass ratio of Ce: MTX was determined to be 2:1, based on particle size, PDI, EE, and LE. The Ce-MTX NPs prepared at this ratio exhibited small, uniform particle sizes, with an EE of 95.15% and 95.74% for Ce and MTX, respectively, demonstrating excellent physicochemical properties.

Characterization of Ce-MTX NPs

The diameter and morphology of Ce-MTX NPs were characterized using DLS and TEM. The particle size distribution plot, Figure 2A and B, shows that the average particle size of Ce-MTX NPs was 90.20 nm, with a PDI of 0.062, and a zeta potential of −35.3 mV (Figure 2A and B). The TEM image (Figure 2C and D) reveals that the particles were spherical and uniformly distributed with an approximate size of 60 nm. This discrepancy in size between TEM and DLS measurements may be due to the solvent layer around the nanoparticles during DLS analysis, leading to a larger hydrodynamic diameter. In the UV absorption spectra, a shift in the maximum absorption wavelength of Ce from 425 nm to 430 nm in Ce-MTX NPs was observed compared to free Ce (Figure 2E). This shift indicated changes in the drug state and the presence of intermolecular interactions within the Ce-MTX NPs. The intermolecular interactions were further supported by FT-IR spectra (Figure 2F). The O-H stretching vibration peaks of Ce at 2926.5 cm^{-1} and 2845.1 cm^{-1} were red-shifted to 2945.6 cm^{-1} and 2870.7 cm^{-1} in Ce-MTX NPs. Additionally, the C=O stretching vibration peak at 1704.7 cm^{-1} in Ce was absent in Ce-MTX NPs. The N-H stretching vibration of MTX (3341.2 cm^{-1}) was broadened and red-shifted to 3419.4 cm^{-1}, likely due to the hydrogen bonding between Ce and MTX. These changes confirmed the intermolecular interactions between Ce and MTX in the nanoparticles. Short-term stability study results show that the particle size of Ce-MTX NPs remained stable in ultrapure water, PBS (pH 7.4) solution, and RPMI-1640 medium (with 10% FBS) for up to 7 days, indicating excellent stability of Ce-MTX NPs (Figure 2G).

In vitro Drug Release of Ce-MTX NPs

To investigate the release behavior of Ce-MTX NPs in different physiological environments, drug release was measured at pH 5.5 (simulating tumor acidic conditions) and pH 7.4 (simulating physiological conditions). As shown in Figure 2H and I, free

Table 1 Solvent Optimization for Ce-MTX NPs (Mean ± SD, n=3)

Solvent	Size (nm)	PDI
Methanol	92.1±2.54	0.104±0.027
Ethanol	167.4±4.85	0.113±0.016
DMSO	174.6±3.74	0.363±0.055

Table 2 Mass Ratio (Ce/MTX) Optimization for Ce-MTX NPs (Mean ± SD, n=3)

Ce/MTX	Size (nm)	PDI	EE/%		LE/%	
			Ce	MTX	Ce	MTX
1:1	113.5±3.84	0.274±0.066	77.41±4.8	85.82±3.3	81.85±0.29	9.86±18.2
2:1	90.22±5.32	0.062±0.014	95.15±1.7	95.74±2.0	66.53±1.86	33.47±1.9
3:1	132.5±3.95	0.102±0.035	89.80±6.7	89.99±3.3	74.96±0.67	25.04±0.67
4:1	155.4±5.23	0.075±0.073	72.07±3.4	91.34±2.5	75.94±0.35	24.06±0.35

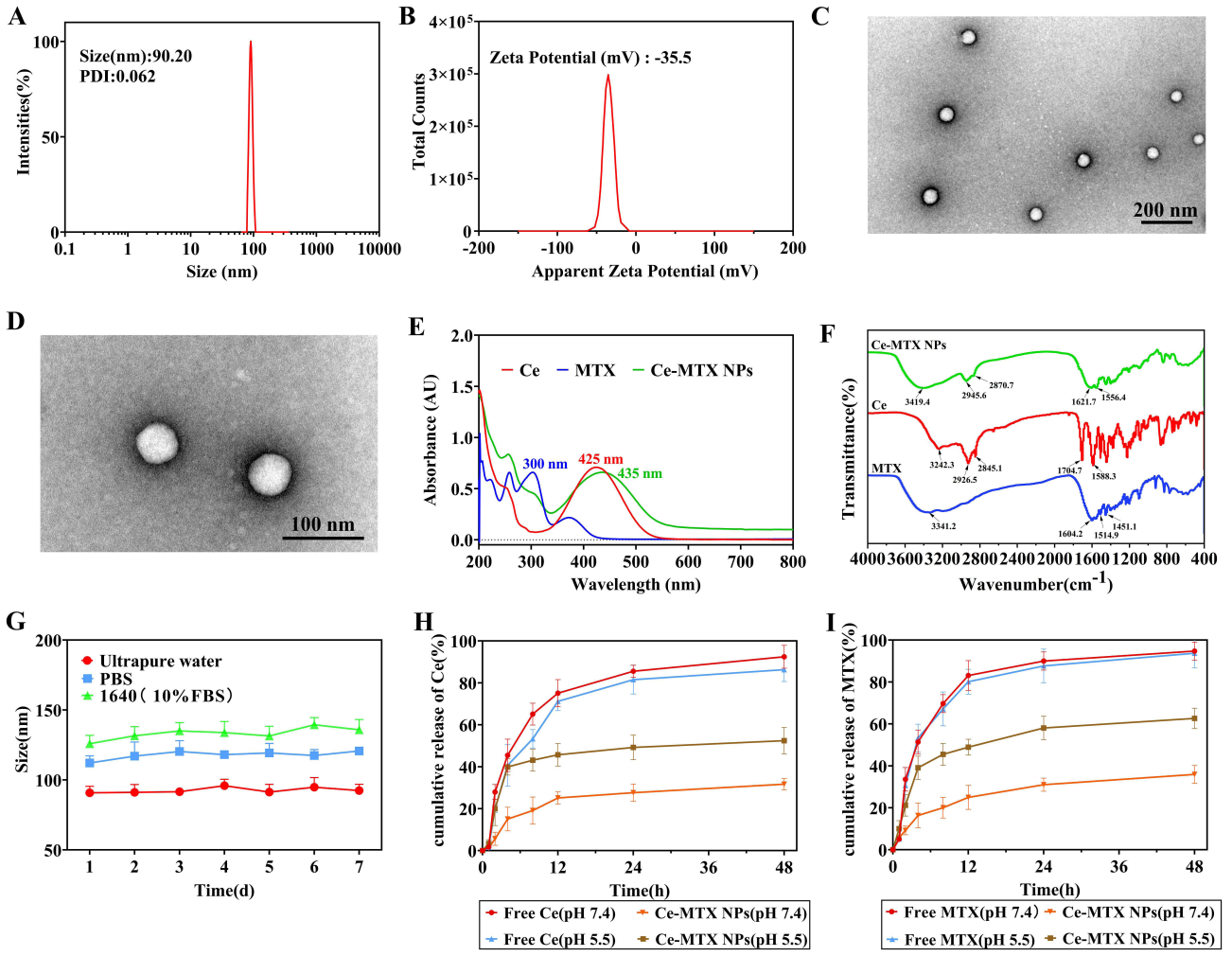

Figure 2 Characterization and drug release of Ce-MTX NPs (**A**) Particle size distribution. (**B**) Zeta potential. (**C**) TEM analysis at 200 nm. (**D**) TEM analysis at 100 nm. (**E**) UV absorption spectra of Ce, MTX, and Ce-MTX NPs. (**F**) FT-IR spectra of Ce, MTX, and Ce-MTX NPs. (**G**) Particle size distribution of Ce-MTX NPs incubated for 7 days in ultrapure water, PBS solution, and 10% fetal calf serum-containing 1640 medium. (**H**) Cumulative drug release profiles of Ce from Ce-MTX NPs at different pH conditions. (**I**) Cumulative drug release profiles of MTX from Ce-MTX NPs at different pH conditions ($\bar{x}$ ± s, n = 3).

Ce and free MTX were rapidly released (> 90%) within 48 hours under both conditions. In contrast, Ce-MTX NPs exhibited a slower, more controlled release, with a noticeable pH dependence. At pH 5.5, approximately 50% of Ce was released within 24 hours, while only about 30% of Ce was released at pH 7.4 (Figure 2H). It was further confirmed that the carrier-free nanoparticles with MTX as an assembly component exhibited pH-dependent release properties. This was attributed to the increased solubility of MTX under acidic conditions, which promoted drug release from the nanoparticles. The above results indicated that the Nps were more stable in the physiological environment and were sensitive to tumors, enabling smooth drug release at the tumor site. Moreover, both Ce and MTX were released simultaneously from Ce-MTX NPs, suggesting their potential for synergistic therapy by enabling the concurrent delivery of both drugs.

Cellular Uptake Assays

The cellular uptake of Ce-MTX NPs by 4T1 and A549 cells was studied by CLSM and flow cytometry. The results are shown in Figure 3A–D. Under identical ICG concentration conditions, 4T1 and A549 cells were incubated for 4 hours in culture media containing different drug formulations. The free ICG group showed lower cell fluorescence intensity in both cell types compared to the Ce-MTX-ICG NPs group. This difference can be attributed to the fact that free ICG, being a small molecule, enters tumor cells primarily through passive diffusion, resulting in limited uptake. In contrast, Ce-MTX-ICG NPs were preferentially internalized by tumor cells via folate receptor-mediated endocytosis.[28] In 4T1

https://doi.org/10.2147/IJN.S516921

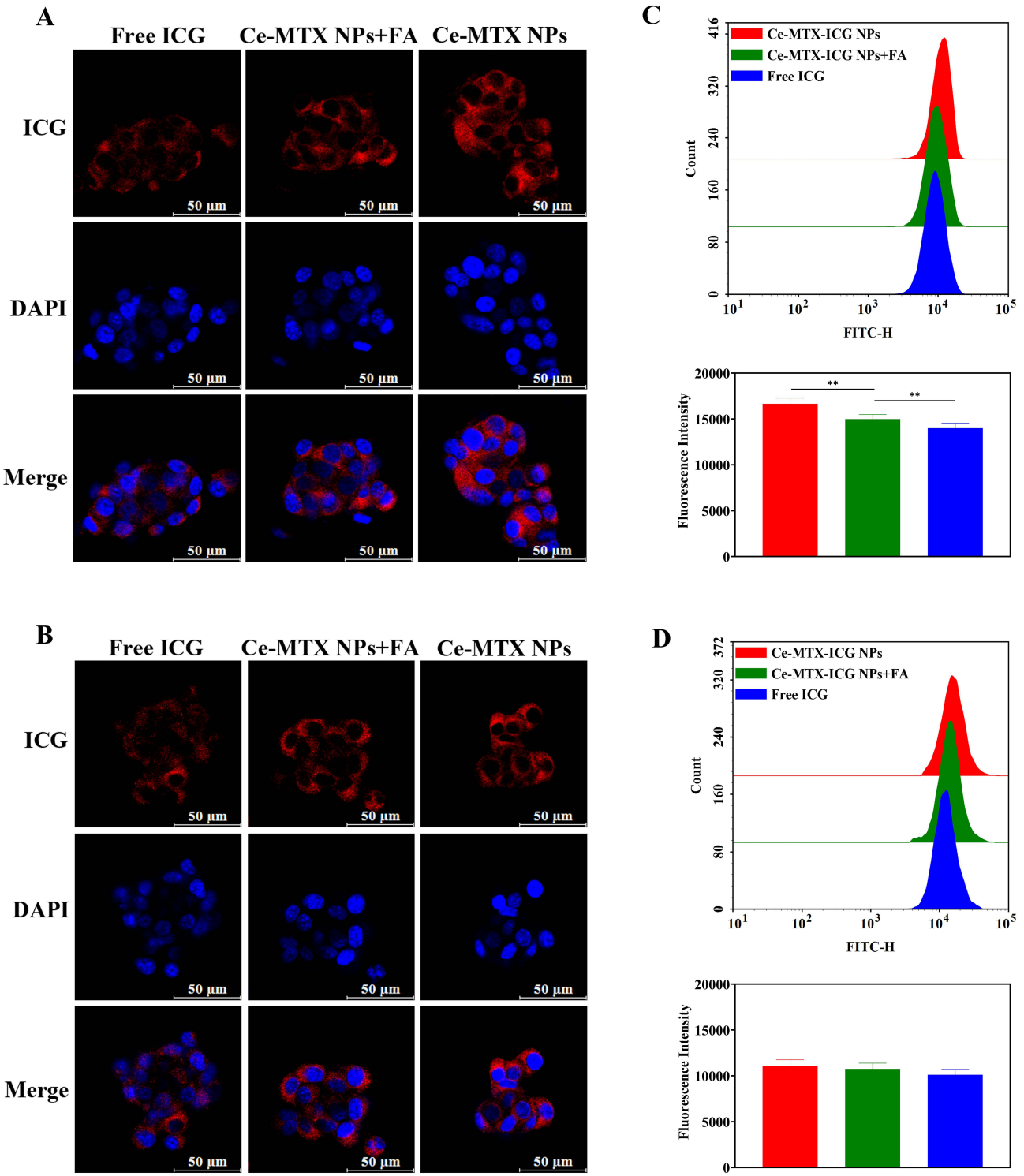

Figure 3 In vitro experiments of cells uptake (**A**) CLSM images of 4T1 cells incubated with free ICG, Ce-MTX-ICG NPs and Ce-MTX-ICG NPs+FA for 4h. (**B**) CLSM images of A549 cells incubated with free ICG, Ce-MTX-ICG NPs and Ce-MTX-ICG NPs+FA for 4h. (**C**) Fluorescence distribution and average fluorescence intensity of free ICG, Ce-MTX-ICG NPs and Ce-MTX-ICG NPs+FA in 4T1. (**D**) Fluorescence distribution and average fluorescence intensity of free ICG, Ce-MTX-ICG NPs and Ce-MTX-ICG NPs+FA in A549.(n=3, $^{**}P<0.01$).

cells, the fluorescence intensity of the Ce-MTX-ICG NPs group was significantly higher than that of the group in which folate receptor activity was blocked by pre-treatment with free FA. This suggests that the uptake of Ce-MTX-ICG NPs was inhibited when the folate receptor was blocked, further supporting the role of folate receptor-mediated endocytosis in nanoparticle uptake. In addition, the fluorescence intensity of the Ce-MTX-ICG NPs group was higher in 4T1 cells than

in A549 cells, indicating that the Ce-MTX-ICG NPs are preferentially taken up by 4T1 cells due to their higher folate receptor expression. These results demonstrate that the self-assembly of Ce with MTX confers targeting properties to the Ce-MTX NPs, facilitating their enhanced uptake by 4T1 mouse mammary carcinoma cells, which overexpress folate receptors.

In vitro Cytotoxicity and Synergistic Effects of Ce-MTX NPs

MTT assay was used to assess the cytotoxicity of Ce-MTX NPs in 4T1 and A549 cells. As shown in Figure 4A–D, the cytotoxicity of free Ce, free MTX, Ce+MTX mixture, and Ce-MTX NPs increased in a concentration and time-dependent manner. Notably, Ce-MTX NPs exhibited significantly higher cytotoxicity compared to the free drug and drug mixtures. For instance, when 4T1 cells were incubated with different treatments (3 μg/mL Ce, 1.5 μg/mL MTX) for 48 hours, the survival rate in the Ce-MTX NPs group was approximately 10%. In contrast, the survival rates were about 20% and 80% in the free Ce and MTX groups, respectively, and around 15% in the Ce+MTX mixture group. After 24 hours of incubation, the IC_{50} values for the free Ce and Ce+MTX mixture groups were 2.169 and 1.298 μg/mL, respectively,

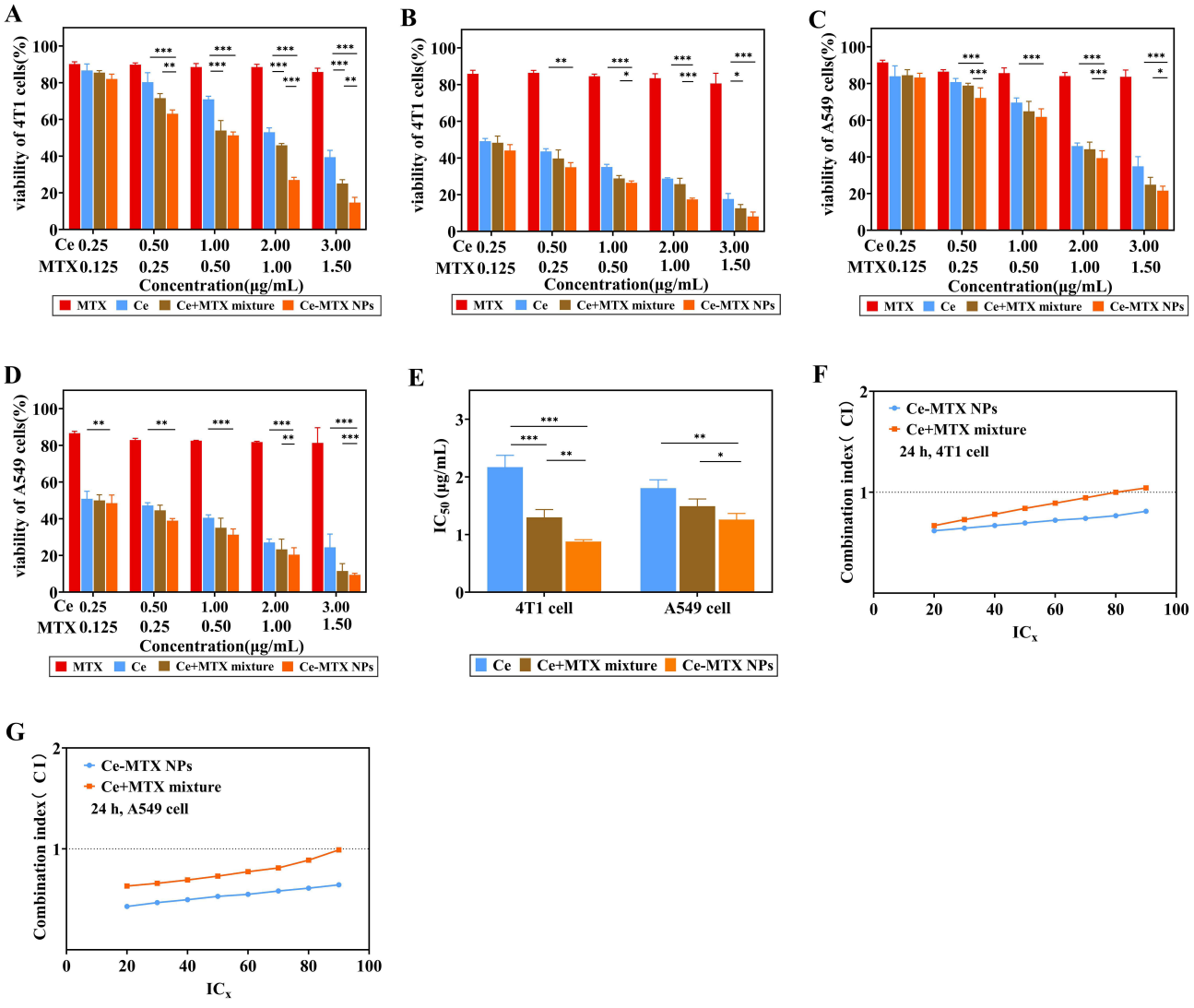

Figure 4 The synergistic effect of Ce and MTX, and the cytotoxicity in vitro. (**A**) Survival rate of 4T1 cells after treatment with varying concentrations for 24 h. (**B**) Survival rate of 4T1 cells after treatment with varying concentrations for 48 h. (**C**) Survival rate of A549 cells after treatment with varying concentrations for 24 h. (**D**) Survival rate of A549 cells after treatment with varying concentrations for 48 h. (**E**) IC_{50} values of free Ce, Ce+MTX mixture, and Ce-MTX NPs in 4T1 and A549 cells. (**F**) Combination index of Ce+MTX mixture and Ce-MTX NPs in 4T1 cells. (**G**) Combination index of Ce+MTX mixture and Ce-MTX NPs in A549 cells. (n=3, **P*<0.05, ***P*<0.01, ****P*<0.001).

https://doi.org/10.2147/IJN.S516921

whereas the IC_{50} value for Ce-MTX NPs was significantly lower at 0.878 μg/mL (Figure 4E). These findings indicated that Ce-MTX NPs significantly enhanced anti-tumor activities compared to the free drug and drug mixtures. Cellular uptake studies revealed that the Ce-MTX NPs were preferentially taken up by tumor cells compared to the free drug; this enhanced uptake contributed to the greater anti-tumor efficacy of Ce-MTX NPs. In addition, MTX-mediated targeting of 4T1 cells resulted in the lowest IC_{50} value, further confirming the efficacy of targeted therapy in improving the anti-tumor effects.

To evaluate the synergistic effects of the Ce+MTX mixture and Ce-MTX NPs, the CI was calculated. As shown in Figure 4F and G, the CI values for the Ce+MTX mixture approached 1 when the inhibition rate (ICx) ranged from 20% to 90%, with the CI value exceeding 1 at IC_{90}. In contrast, the CI values for Ce-MTX NPs were consistently lower than those for the mixture group and remained below 1 across all inhibition rates. This suggested that Ce-MTX NPs exhibited a more pronounced synergistic effect than the free drug mixture, indicating superior anti-tumor activity. The enhanced synergy observed with Ce-MTX NPs can be attributed to the self-assembled nanosystem, which enables the efficient co-delivery of Ce and MTX to tumor cells. Intermolecular interactions within the nanoparticles facilitated the synchronous release of both drugs, thereby optimizing their therapeutic effects. These results highlight the improved cytotoxicity and synergistic anti-tumor efficacy of Ce-MTX NPs compared to the free drug mixture.

In vivo Distribution of Ce-MTX NPs

4T1 tumor-bearing mice were selected to evaluate the in vitro and in vivo distribution of ICG at different time points, following the injection of free ICG and Ce-MTX-ICG NPs via the tail vein. Near-infrared fluorescence imaging was employed to track the distribution. As shown in Figure 5A, the fluorescence intensity of free ICG decreased rapidly over time, nearly disappearing by 24 hours. In contrast, the Ce-MTX-ICG NPs exhibited a gradual accumulation of fluorescence in the tumor, with the intensity stabilizing after 12 hours and remaining consistent for up to 48 hours. The results suggested that Ce-MTX NPs enhance targeting and improve the retention time of the drug in vivo.

To further understand the metabolism and accumulation of the NPs at the tumor site, ex vivo fluorescence imaging of mouse organs and tumors was conducted at 48 hours post-injection. The results demonstrated that the fluorescence was predominantly localized in the liver and the tumor (Figure 5A). Notably, Ce-MTX-ICG NPs displayed higher fluorescence intensity in the liver and significant accumulation at the tumor site within the 48-hour period. This finding confirmed that Ce-MTX NPs exhibited effective retention at the tumor site, primarily through the EPR effect, along with folate receptor-mediated targeting, which facilitated drug accumulation and improved anti-tumor efficacy.

Additionally, the high fluorescence intensity observed in the liver may indicate the involvement of the liver in the metabolic pathway of Ce-MTX NPs. This warrants further investigation to assess potential effects on liver function.

In vivo Anti-Tumor Effects of Ce-MTX NPs

To further evaluate the anti-tumor efficacy of Ce-MTX NPs, a 4T1 tumor-bearing mouse model was used. Mice were treated with Ce-MTX NPs, and body weight and tumor volume were measured every two days. As shown in Figure 5B, the body weights of mice in all groups remained within the normal range, indicating that the NPs did not cause significant toxic side effects. Figure 5C illustrates that the tumor volume in the Ce-MTX NPs group was significantly smaller compared to the other groups. At the end of the treatment cycle, tumors and organs were excised, and both organ indices and tumor inhibition rates were calculated. Tumor weights and volumes in the Ce-MTX NPs group were significantly reduced than those of the free drug and mixture groups (Figure 5D and E), resulting in a higher tumor inhibition rate (Figure 5F). Although the Ce+MTX mixture group exhibited synergistic effects in the cytotoxicity assay, its therapeutic efficacy was limited. This is likely due to the inability of the free drugs to effectively accumulate at the tumor site during circulation, as the two drugs have distinct in vivo distributions. In contrast, Ce-MTX NPs, through the enhanced permeability and retention (EPR) effect and folate receptor-mediated targeting, demonstrated superior tumor site accumulation, leading to more effective synergistic antitumor effects.

Organ index analysis (Figure 6A) demonstrated no significant changes in the heart, liver, spleen, or lung in any group. However, the renal index in the Ce+MTX mixture group was higher than in the Ce-MTX NPs group ($p < 0.05$),

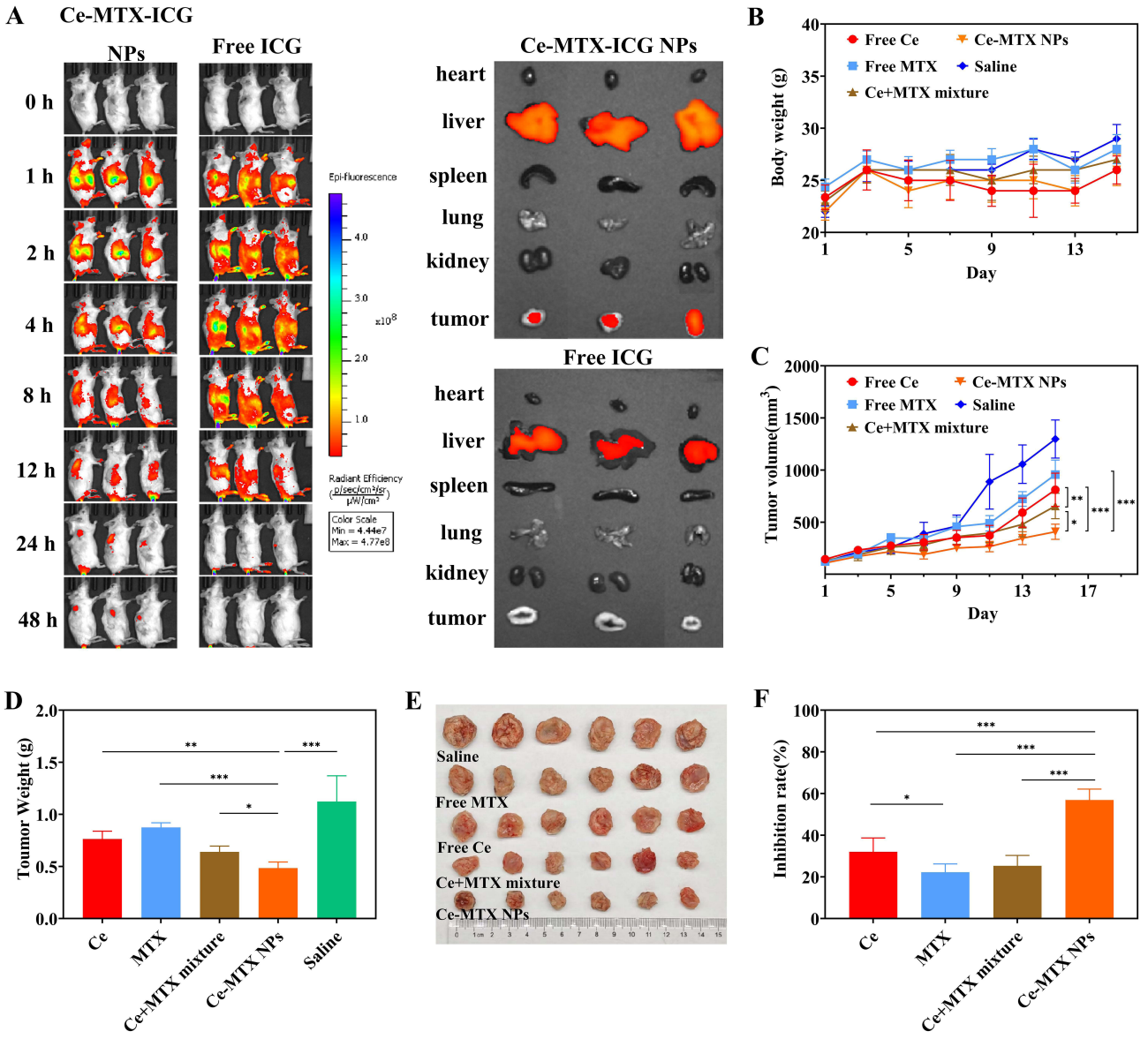

Figure 5 In vivo anti-tumor study of Ce-MTX NPs in 4T1 tumor-bearing mice (**A**) In vivo and ex vivo NIR fluorescence distribution of major organs and tumors following intravenous injection of free ICG or Ce-MTX-ICG NPs. (**B**) Body weight changes of mice in each group. (**C**) Tumor volume changes in each group. (**D**) Average tumor weight of each group. (**E**) Tumor images after 15 days of treatment. (**F**) Tumor inhibition rate in each group. (n=3, **P*<0.05, ***P*<0.01, ****P*<0.001).

suggesting that the combination of free Ce and MTX may cause renal toxicity. These results imply that Ce-MTX NPs can mitigate the renal damage associated with free drugs.

Histopathological analysis of tumor and organ tissues further assessed the antitumor efficacy and biosafety of Ce-MTX NPs. As shown in Figure 6B, kidney sections from the free Ce and Ce+MTX mixture groups exhibited varying degrees of inflammatory cell infiltration, indicative of nephrotoxicity induced by free Ce.[29] However, no significant pathological damage was observed in other organ tissues. These results strongly indicate that Ce-MTX NPs can effectively reduce the systemic toxicity associated with free drug treatment.

To further evaluate the toxicity of each treatment group, serum levels of AST, ALT, BUN, and CRE were measured as indicators of liver and kidney function. Figure 6C and D show that there were no significant differences in ALT and AST levels between the groups, indicating no major liver toxicity. CRE levels were within the normal range across all groups. However, BUN levels in the free Ce and Ce+MTX mixture groups were elevated compared to the other groups, suggesting some kidney damage, which was consistent with the pathological findings. In contrast, there were no

https://doi.org/10.2147/IJN.S516921

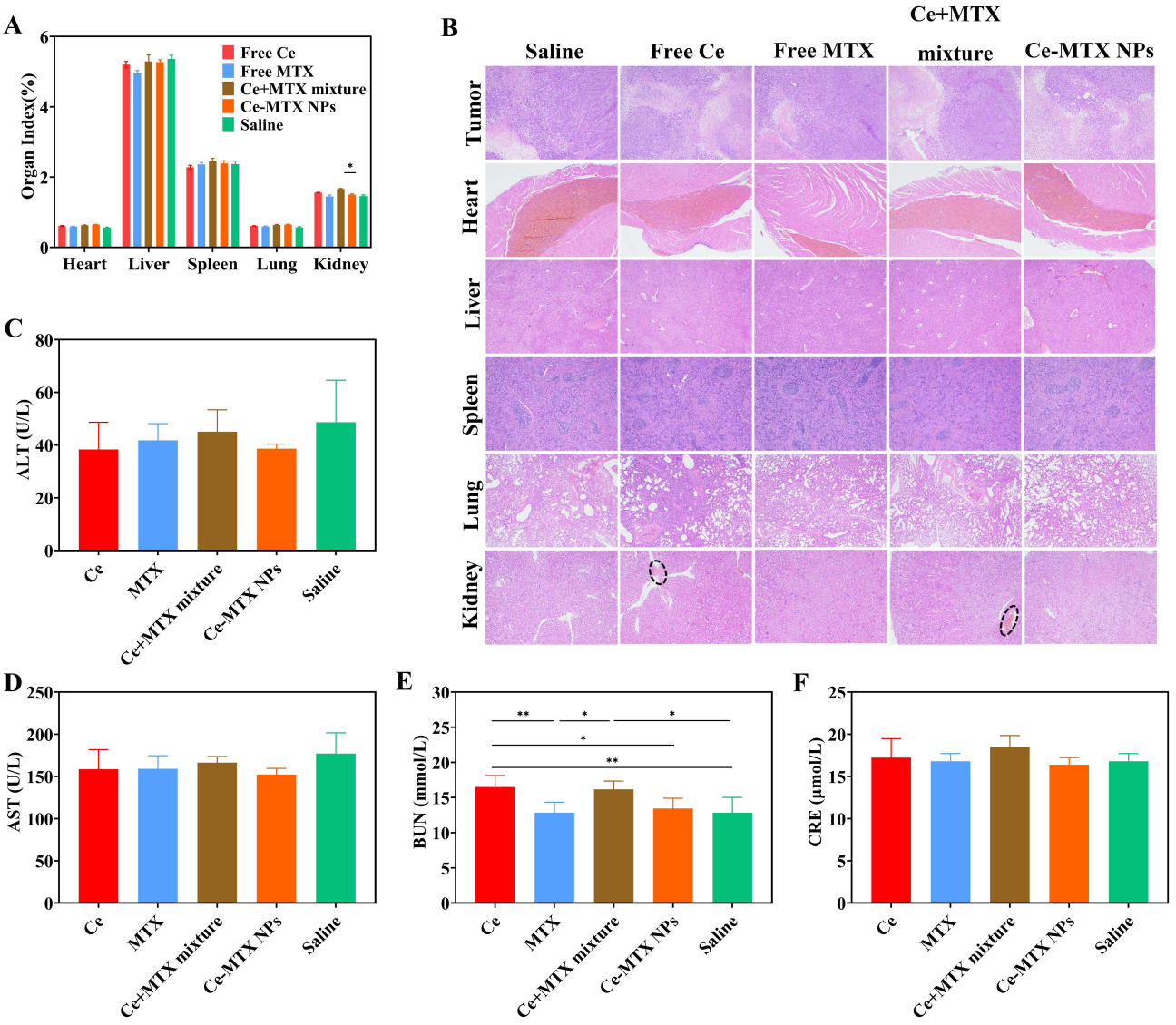

Figure 6 In vivo safety evaluation of Ce-MTX NPs in 4T1 tumor-bearing mice (**A**) Organ index of mice. (**B**) Histopathological sections of organs. (**C** and **D**) Serum liver function: ALT and AST levels. (**E** and **F**) Serum renal function: BUN and CRE levels. (n=6, **P*<0.05, ***P*<0.01).

significant changes in BUN levels in the Ce-MTX NPs group compared to the control, further indicating that Ce-MTX NPs effectively reduced free Ce-induced nephrotoxicity (Figure 6E and F). The reduction in toxicity is mainly attributed to two factors: First, Ce-MTX NPs have excellent passive and active tumor-targeting properties, thereby significantly reducing drug distribution in normal tissues. Second, its sustained-release property in normal physiological environments also reduces the impact on normal tissues. Overall, these characteristics highlight the great potential of Ce-MTX NPs for anti-tumor therapy.

Conclusion

In this study, we developed a carrier-free nanoparticle formulation combining Ce and MTX, which not only has excellent tumor-targeting ability but also achieves the synergistic anticancer effects of the two drugs. Characterization of Ce-MTX NPs demonstrated that the NPs exhibited a uniform spherical morphology with high drug EE and LE.In addition, Ce-MTX NPs were capable of efficiently releasing the drugs in acidic tumor environments. Cellular uptake assays showed that Ce-MTX NPs significantly enhanced the uptake of Ce and MTX by tumor cells that express high levels of folate receptors. Cytotoxicity assays further demonstrated that Ce-MTX NPs exhibited excellent synergistic effects and potent

tumor cell-killing activity. In vivo studies showed that Ce-MTX NPs effectively prolonged the circulation time and promoted its targeted accumulation at the tumor site. The Ce-MTX NPs significantly improved the antitumor efficacy of both Ce and MTX while showing favorable biocompatibility. In conclusion, the study presents a promising strategy for the treatment of breast cancer using Ce-MTX NPs, demonstrating strong potential for further development in cancer therapy.

Ethics Approval and Consent to Participate

In this study, all methods were carried out in accordance with relevant guidelines and regulations. The Animal Management Committee of Fujian University of Traditional Chinese Medicine approved the protocols used in this study. All procedures involving animals were performed in compliance with animal protection laws and ethical guidelines.

Disclosure

The authors declare no conflicts of interest related to this work.

References

1. Bray F, Ferlay J, Soerjomataram I, Siegel RL, Torre LA, Jemal A. Global cancer statistics 2018: GLOBOCAN estimates of incidence and mortality worldwide for 36 cancers in 185 countries. *CA Cancer J Clin*. 2018;68(6):394–424. doi:10.3322/caac.21492
2. Ashrafizadeh M, Zarrabi A, Bigham A, et al. (Nano)platforms in breast cancer therapy: drug/gene delivery, advanced nanocarriers and immunotherapy. *Med Res Rev*. 2023;43(6):2115–2176. doi:10.1002/med.21971
3. LRF LRF. Twenty Years of Advancing Discoveries and Treatment of Mantle Cell Lymphoma. *Oncology*. 2024;38(2):51–67. doi:10.46883/2024.25921013
4. Ji N, Li J, Wei Z, et al. Effect of celastrol on growth inhibition of prostate cancer cells through the regulation of hERG channel in vitro. *Biomed Res Int*. 2015;2015:308475. doi:10.1155/2015/308475
5. Shen B, Chen HB, Zhou HG, Wu MH. Celastrol induces caspase-dependent apoptosis of hepatocellular carcinoma cells by suppression of mammalian target of rapamycin. *J Tradit Chin Med*. 2021;41(3):381–389. doi:10.19852/j.cnki.jtcm.2021.03.006
6. Qin JJ, Niu MD, Cha Z, et al. TRAIL and Celastrol Combinational Treatment Suppresses Proliferation, Migration, and Invasion of Human Glioblastoma Cells via Targeting Wnt/β-catenin Signaling Pathway. *Chin J Integr Med*. 2024;30(4):322–329. doi:10.1007/s11655-023-3752-7
7. Gan X, Wang F, Luo J, et al. Proteolysis Targeting Chimeras (PROTACs) based on celastrol induce multiple protein degradation for triple-negative breast cancer treatment. *Eur J Pharm Sci*. 2024;192:106624. doi:10.1016/j.ejps.2023.106624
8. He P, Zou M, Zhang C, Shi Y, Qin L. Celastrol-Loaded Hyaluronic Acid/Cancer Cell Membrane Lipid Nanoparticles for Targeted Hepatocellular Carcinoma Prevention. *Cells*. 2024;13(21):1819. doi:10.3390/cells13211819
9. Huang S, Xiao S, Li X, et al. Development of Dual-Targeted Mixed Micelles Loaded with Celastrol and Evaluation on Triple-Negative Breast Cancer Therapy. *Pharmaceutics*. 2024;16(9):1174. doi:10.3390/pharmaceutics16091174
10. Chen Y, Zhang Z, Qian Z, Ma R, Luan M, Sun Y. Sequentially Released Liposomes Enhance Anti-Liver Cancer Efficacy of Tetrandrine and Celastrol-Loaded Coix Seed Oil. *Int J Nanomed*. 2024;19:727–742. doi:10.2147/ijn.S446895
11. Wang F, Lai W, Xie D, et al. Nanoparticle-mediated celastrol ER targeting delivery amplify immunogenic cell death in melanoma. *J Adv Res*. 2024;2024:2. doi:10.1016/j.jare.2024.06.011
12. Alkhaldi O, Abusulieh S, Abusara OH, Sunoqrot S. Development of Mitoxantrone-Loaded Quercetin Nanoparticles for Breast Cancer Therapy with Potential for Synergism with Bioactive Natural Products. *Int J Pharm*. 2024;665:124674. doi:10.1016/j.ijpharm.2024.124674
13. Bhirud D, Bhattacharya S, Raval H, et al. Chitosan nanoparticles of imatinib mesylate coated with TPGS for the treatment of colon cancer: in-vivo & in-vitro studies. *Carbohydr Polym*. 2025;348(Pt B):122935. doi:10.1016/j.carbpol.2024.122935
14. Li Y, Lin J, Ma J, et al. Methotrexate-Camptothecin Prodrug Nanoassemblies as a Versatile Nanoplatform for Biomodal Imaging-Guided Self-Active Targeted and Synergistic Chemotherapy. *ACS Appl Mater Interfaces*. 2017;9(40):34650–34665. doi:10.1021/acsami.7b10027
15. Zhang Y, Fang F, Li L, Zhang J. Self-Assembled Organic Nanomaterials for Drug Delivery, Bioimaging, and Cancer Therapy. *ACS Biomater Sci Eng*. 2020;6(9):4816–4833. doi:10.1021/acsbiomaterials.0c00883
16. Xiao H, Guo Y, Liu H, et al. Structure-based design of charge-conversional drug self-delivery systems for better targeted cancer therapy. *Biomaterials*. 2020;232:119701. doi:10.1016/j.biomaterials.2019.119701
17. Xiao Y, Liu J, Guo M, et al. Synergistic combination chemotherapy using carrier-free celastrol and doxorubicin nanocrystals for overcoming drug resistance. *Nanoscale*. 2018;10(26):12639–12649. doi:10.1039/c8nr02700e
18. Liu H, Nie T, Duan X, et al. Cerebral delivery of redox-responsive lenalidomide prodrug plus methotrexate for primary central nerve system lymphoma combination therapy. *J Control Release*. 2023;359:132–146. doi:10.1016/j.jconrel.2023.05.040
19. Bajracharya R, Baral KC, Lee SH, Song JG, Han HK. Organometallic Phyllosilicate-Gold Nanocomplex: an Effective Oral Delivery System of Methotrexate for Enhanced in vivo Efficacy Against Colorectal Cancer. *Int J Nanomed*. 2023;18:7257–7266. doi:10.2147/ijn.S437860
20. Syed A, Baker A, Mohany M, Elgorban AM, Khan MS, Al-Rejaie SS. IgG antibodies mediated gold nanoparticles conjugated to methotrexate as targeted chemotherapy for lung cancer. *Artif Cells Nanomed Biotechnol*. 2023;51(1):384–396. doi:10.1080/21691401.2023.2242419
21. Bhattacharya S, Prajapati BG, Ali N, Mohany M, Aboul-Soud MAM, Khan R. Therapeutic Potential of Methotrexate-Loaded Superparamagnetic Iron Oxide Nanoparticles Coated with Poly(lactic-co-glycolic acid) and Polyethylene Glycol against Breast Cancer: development. *Characterization, and Comprehensive in Vitro Investigation ACS Omega*. 2023;8(30):27634–27649. doi:10.1021/acsomega.3c03430

22. Cronstein BN, Aune TM. Methotrexate and its mechanisms of action in inflammatory arthritis. *Nat Rev Rheumatol*. 2020;16(3):145–154. doi:10.1038/s41584-020-0373-9
23. Zhang H, Li Y, Pan Z, et al. Multifunctional Nanosystem Based on Graphene Oxide for Synergistic Multistage Tumor-Targeting and Combined Chemo-Photothermal Therapy. *Mol Pharm*. 2019;16(5):1982–1998. doi:10.1021/acs.molpharmaceut.8b01335
24. Siddique MY, Zafar S, Rizwan L, et al. Formulation and structural insight of biocompatible microemulsion for enhanced release profile of anticancer methotrexate. Original Research. *Front Mater*. 2024;11:1.
25. Farshbaf M, Salehi R, Annabi N, Khalilov R, Akbarzadeh A, Davaran S. pH- and thermo-sensitive MTX-loaded magnetic nanocomposites: synthesis, characterization, and in vitro studies on A549 lung cancer cell and MR imaging. *Drug Dev Ind Pharm*. 2018;44(3):452–462. doi:10.1080/03639045.2017.1397686
26. Noreen S, Hasan S, Ghumman SA, et al. pH Responsive Abelmoschus esculentus Mucilage and Administration of Methotrexate: in-Vitro Antitumor and In-Vivo Toxicity Evaluation. *Int J Mol Sci*. 2022;23(5):2725. doi:10.3390/ijms23052725
27. Gipson K, Kucera C, Stadther D, Stevens K, Ballato J, Brown P. The Influence of Synthesis Parameters on Particle Size and Photoluminescence Characteristics of Ligand Capped Tb3+:LaF3. *Polymers*. 2011;3(4):2039–2052. doi:10.3390/polym3042039
28. Ahmadi M, Ritter CA, von Woedtke T, Bekeschus S, Wende K. Package delivered: folate receptor-mediated transporters in cancer therapy and diagnosis. *Chem Sci*. 2024;15(6):1966–2006. doi:10.1039/d3sc05539f
29. Wu M, Chen W, Yu X, et al. Celastrol aggravates LPS-induced inflammation and injuries of liver and kidney in mice. *Am J Transl Res*. 2018;10(7):2078–2086.